Journal of Zhejiang University-SCIENCE B (Biomedicine & Biotechnology) 2025 26(5):461-476
www.jzus.zju.edu.cn; www.springer.com/journal/11585
E-mail: jzus_b@zju.edu.cn

Research Article
https://doi.org/10.1631/jzus.B2300825

Check for updates

Pharmacological inhibition of ENaC or NCX can attenuate hepatic ischemia-reperfusion injury exacerbated by hypernatremia

Yabin CHEN[1], Hao LI[2], Peihao WEN[1], Jiakai ZHANG[1], Zhihui WANG[1], Shengli CAO[1], Wenzhi GUO[1]✉

[1]*Department of Hepatobiliary and Pancreatic Surgery, The First Affiliated Hospital of Zhengzhou University, Zhengzhou 450052, China*
[2]*Henan Organ Transplantation Centre, Zhengzhou 450052, China*

Abstract: Donors with a serum sodium concentration of >155 mmol/L are extended criteria donors for liver transplantation (LT). Elevated serum sodium of donors leads to an increased incidence of hepatic dysfunction in the early postoperative period of LT; however, the exact mechanism has not been reported. We constructed a Lewis rat model of 70% hepatic parenchymal area subjected to ischemia-reperfusion (I/R) with hypernatremia and a BRL-3A cell model of hypoxia-reoxygenation (H/R) with high-sodium (HS) culture medium precondition. To determine the degree of injury, biochemical analysis, histological analysis, and oxidative stress and apoptosis detection were performed. We applied specific inhibitors of the epithelial sodium channel (ENaC) and Na^+/Ca^{2+} exchanger (NCX) in vivo and in vitro to verify their roles in injury. Serum alanine aminotransferase (ALT), aspartate aminotransferase (AST), and lactate dehydrogenase (LDH) levels and the area of hepatic necrosis were significantly elevated in the HS+I/R group. Increased reactive oxygen species (ROS) production, myeloperoxidase (MPO)-positive cells, and aggravated cellular apoptosis were detected in the HS+I/R group. The HS+H/R group of BRL-3A cells showed significantly increased cellular apoptosis and ROS production compared to the H/R group. The application of amiloride (Amil), a specific inhibitor of ENaC, reduced ischemia-reperfusion injury (IRI) aggravated by HS both in vivo and in vitro, as evidenced by decreased serum transaminases, inflammatory cytokines, apoptosis, and oxidative stress. SN-6, a specific inhibitor of NCX, had a similar effect to Amil. In summary, hypernatremia aggravates hepatic IRI, which can be attenuated by pharmacological inhibition of ENaC or NCX.

Key words: Liver transplantation; Epithelial sodium channel (ENaC); Na^+/Ca^{2+} exchanger (NCX); Hypernatremia

1 Introduction

Liver transplantation (LT) is an effective treatment for various end-stage liver diseases, and the livers are mainly derived from brain-dead donors (Guo et al., 2023; Schlegel et al., 2023). Shortage of donor livers is one of the dilemmas facing LT, and expanding the source of donor livers has become critical, with more and more extended-criteria donor livers being used in transplantation (Ceresa et al., 2022; Sitbon et al., 2023). Extended-criteria donor livers are those with a high risk of primary graft nonfunction or hypofunction and delayed graft inactivation after transplantation. A donor with a serum sodium concentration of >155 mmol/L (hypernatremia donor) would be considered an extended criteria donor (Basmaji et al., 2020; Lin et al., 2023). It has been proven that the use of livers from hypernatremia donors leads to an increased incidence of poor liver function in the short-term postoperative period, and some studies also have reported elevated postoperative mortality of recipients (Bastos-Neves et al., 2019; Basmaji et al., 2020; Zhou et al., 2020; McDonald et al., 2021).

Ischemia-reperfusion injury (IRI) is an important cause of postoperative hepatic dysfunction. During periods of liver ischemia, the lack of oxygen and energy supply to hepatocytes leads to metabolic abnormalities and the release of danger-associated molecular patterns (DAMPs) (Kaltenmeier et al., 2022; Lucas-Ruiz et al., 2023). After the blood supply is restored, the reintroduction of oxygen supply increases the production of reactive oxygen species (ROS), which further aggravates cellular damage and inflammatory

✉ Wenzhi GUO, fccguowz@zzu.edu.cn
Wenzhi GUO, https://orcid.org/0000-0002-0821-1318

Received Nov. 14, 2023; Revision accepted Apr. 22, 2024; Crosschecked May 27, 2025

responses (Dar et al., 2019). However, the mechanism by which hypernatremia aggravates hepatic IRI has not been reported.

Epithelial sodium channel (ENaC) is a type of sodium channel that is widely distributed in multiple organs, and mainly mediates cellular sodium transport (Chen et al., 2023). Hypernatremia aggravates renal IRI through ENaC. Amiloride (Amil) can reduce the expression of ENaC and attenuate hypernatremia-aggravated renal IRI (Matsumoto et al., 2022). The expression of Na^+/Ca^{2+} exchanger (NCX) is increased after myocardial ischemia-reperfusion (I/R), and SN-6 can decrease the expression of NCX and be applied to reduce myocardial IRI (Castaldo et al., 2017). Activation of the ENaC-NCX-NLRP3 (NOD-like receptor family, pyrin domain-containing 3) signaling pathway can lead to increased ROS production and exacerbated inflammatory responses, which has been reported in many diseases such as cystic fibrosis (Scambler et al., 2019) and salt-sensitive hypertension (Chen et al., 2021; Pitzer et al., 2022). Therefore, we hypothesized that hypernatremia aggravates hepatic IRI through the activation of ENaC and NCX.

2 Materials and methods

2.1 Animals

Male Lewis rats (6–8 weeks) were purchased from Beijing Viton Lihua Laboratory Animal Technology Co. (Beijing, China). All rats were housed in (25±2) ℃ and (55±5)% humidity environment with a 12-h dark/light cycle. All the rats were acclimatized for one week prior to the experiment.

2.2 Rat models and drug treatment

For the I/R rat model, a 70% liver warm I/R model was established as previously described. Briefly, Lewis rats were anesthetized with sodium pentobarbital, and the abdominal wall was clipped longitudinally. The arteries, portal veins, and bile ducts of the left and middle lobes of the livers were clamped with vascular clips for 1 h, followed by reperfusion for 6 h. Then, the rats were sacrificed, and specimens were obtained (Guo et al., 2020; Li et al., 2023).

For the high-sodium (HS) rat model, Lewis rats were anesthetized, and a HS solution was pumped via tail vein cannulation. Firstly, 0.7 mL of 3 mol/L NaCl solution per 100 g body weight (BW) was rapidly pumped over 5 min. Then, 0.7 mL/h of 3 mol/L NaCl solution was continuously pumped for 3 h, followed by 0.2 mL/h of 3 mol/L NaCl solution continuously pumped for 6 h. Blood was drawn intermittently via femoral artery cannulation for the detection of serum sodium concentration.

For the HS+I/R rat model, the pumping of the HS solution was stopped after establishing the HS rat model, and then the establishment of the I/R model was followed by intermittent oral feeding of a 20% (0.2 g/mL) glucose solution and subcutaneous injection of sodium pentobarbital.

For the Amil+I/R rat model, prior to establishing the I/R model, rats were injected intraperitoneally with Amil (HY-B0285A, MedChemExpress, Monmouth Junction, NJ, USA) at 1 mg/kg BW (Quansah and N'Gouemo, 2014; Frindt et al., 2018). The SN-6+I/R rat model was established in the same way, with SN-6 (HY-107658, MedChemExpress) at 1 mg/kg BW (N'Gouemo, 2013; Quansah and N'Gouemo, 2014; Persaud et al., 2022). For the Amil+HS+I/R rat model, rats were injected intraperitoneally with Amil at 1 mg/kg BW prior to establishing the HS+I/R model, while the SN-6+HS+I/R rat model was established in the same way with SN-6 at 1 mg/kg BW.

2.3 Cell culture and cell models

BRL-3A cells (Cellverse, Shanghai, China) were cultured with Dulbecco's modified Eagle's medium (DMEM; Solarbio, Beijing, China) supplemented with 10% (volume fraction) fetal bovine serum (Gibco, Grand Island, NY, USA) under normal conditions (5% CO_2 and water-saturated incubator at 37 ℃). For the HS cell model, the sodium concentration of the culture medium was 190 mmol/L.

For the hypoxia-reoxygenation (H/R) cell model, the medium was changed to serum-free and glucose-free DMEM, and the cells were transferred to a modular incubator chamber (BioSpherix, Lacona, NY, USA) under hypoxic conditions (1% O_2, 5% CO_2, and 94% N_2). After 6 h of hypoxia, the cells were transferred into a normoxic incubator (95% air+5% CO_2 mixture) for reoxygenation for 6 h, and the medium was changed to a complete medium. For the HS+H/R cell model, the cells were first cultured in 190 mmol/L HS medium for 24 h, followed by H/R conditions (Guo et al., 2020; Ding et al., 2022).

For the Amil+H/R cell model, the cells were first cultured in a culture medium containing 10 μmol/L

Amil, followed by H/R conditions, while the SN-6+ H/R cell model was established with 10 μmol/L SN-6. For the Amil+HS+H/R cell model, the cells were cultured in 190 mmol/L HS medium containing 10 μmol/L Amil, followed by H/R conditions, while the SN-6+ HS+H/R cell model was established with 10 μmol/L SN-6.

2.4 Biochemical analysis

Serum alanine aminotransferase (ALT), aspartate aminotransferase (AST), and lactate dehydrogenase (LDH) in the serum of the rats were tested using commercial kits (Jiancheng Bioengineering Institute, Nanjing, China) according to the manufacturer's instructions.

2.5 Cell-counting kit-8 assay

BRL-3A cells were seeded into 96-well plates at a density of 5×10^3 cells/well, and subjected to different treatments followed by hypoxia for 6 h and reoxygenation for 6 h. Then, according to the instructions of the cell-counting kit-8 (CCK-8; Boster, Wuhan, China), 10 μL of CCK-8 reagent was added to each well. The absorbance of each well was measured at 450 nm after being incubated for 1 h at 37 ℃.

2.6 Histological and immunohistochemical staining

All hepatic tissues were fixed in 10% (volume fraction) formaldehyde solution and embedded in paraffin. Then, the tissues were cut into 5-μm sections. Paraffin sections were stained with hematoxylin and eosin (H&E; Servicebio, Wuhan, China) for staining. Myeloperoxidase (MPO) antibody (volume dilution ratio 1∶100) (Servicebio, Wuhan, China) and secondary antibody (1∶200) (Servicebio, Wuhan, China) were incubated for immunohistochemical staining. The images were photographed using an inverted optical microscope (Olympus, Tokyo, Japan).

2.7 Flow cytometry analysis

After discarding the medium, the BRL-3A cells were washed twice with phosphate-buffered saline (PBS), then digested with ethylenediaminetetraacetic acid (EDTA)-free trypsin (Beyotime, Shanghai, China), collected, and centrifuged at 200*g* for 5 min. Next, 100 μL binding buffer, 5 μL Annexin V-fluorescein isothiocyanate (FITC), and 5 μL propidium iodide (Beyotime) were added to resuspend and stain the cells before incubating them at room temperature for 15 min in the dark; finally, apoptosis was analyzed by flow cytometry.

2.8 Western blot analysis

Protein expression levels in hepatic tissues and cells were detected by western blot analysis according to standard protocols. Radio-immunoprecipitation assay (RIPA) lysis buffer (Solarbio) was used to extract proteins, and a bicinchoninic acid (BCA) kit (Solarbio) was used to quantify the concentrations of proteins. The proteins were separated by 10% or 12% (0.10 or 0.12 g/mL) sodium dodecyl sulfate-polyacrylamide gel electrophoresis (SDS-PAGE), and then transferred to polyvinylidene fluoride (PVDF) membranes. The PVDF membranes were incubated with the specific primary antibody at 4 ℃ overnight, followed by the secondary antibody at 37 ℃ for 1 h. All the antibodies' information is listed in Table S1. The electrochemiluminescence (ECL) reagent (NCM Biotech, Suzhou, China) was used, and the signals were visualized using the ChemiDoc™ MP Imaging System (Bio-Rad, Hercules, CA, USA).

2.9 qPCR

TRIzol reagent (Invitrogen, Carlsbad, CA, USA) was used to extract total RNA from the hepatic tissues and BRL-3A cells. After reverse transcription of RNA to complementary DNA (cDNA), quantitative real-time polymerase chain reaction (qPCR) was performed based on the instructions of SYBR qPCR Master Mix reagent (Vazyme, Nanjing, China). Glyceraldehyde 3-phosphate dehydrogenase (*GAPDH*) was used as the internal reference gene; the primer sequences for target gene amplification are listed in Table S2.

2.10 Oxidative stress analysis

Hepatic tissue specimens were rapidly frozen and fixed; then, the specimens were cut into 10-μm sections and stained with 10 μmol/L dihydroethidium (DHE; Servicebio, Wuhan, China) and 4',6-diamidino-2'-phenylindol (DAPI; Servicebio) fluorescent probes. After grinding the hepatic tissues, the protein concentration was determined by BCA, and the levels of malondialdehyde (MDA), superoxide dismutase (SOD), and glutathione (GSH) (Solarbio) in the tissues were determined according to the manufacturer's instructions. After removing the medium and washing the

cells twice with PBS, ROS (Biosharp, Hefei, China) and DAPI were added to the BRL-3A cells according to the instructions and were photographed using a fluorescence microscope (Olympus).

2.11 TUNEL assay

Paraffin-embedded hepatic tissues were cut into 5 μm-thick sections and then stained according to the instructions of the terminal deoxynucleotidyl transferase dUTP nick-end labeling (TUNEL) kit (Servicebio). DAPI was used to stain the nuclei in the sections, followed by the application of an anti-fluorescence quenching solution (Servicebio). The images were captured using a fluorescence microscope (Olympus).

2.12 Statistical analysis

All data were analyzed using SPSS software (version 27.0) and expressed as mean±standard deviation (SD). The Student's *t*-test was used to compare two groups, while one-way analysis of variance (ANOVA) was used to compare multiple groups. $P<0.05$ was considered statistical significance.

3 Results

3.1 Effect of hypernatremia on hepatic IRI in Lewis rats

To study the effect of hypernatremia on hepatic IRI, we constructed an HS+I/R Lewis rat model by intravenously pumping 3 mol/L NaCl and using 70% of liver I/R (Fig. 1a). Serum results showed that the ALT, AST, and LDH levels of rats in the HS+I/R group were significantly elevated compared to those in the I/R group (Figs. 1b–1d), and the hepatic necrotic area in the HS+I/R group was significantly expanded as shown in the H&E-stained images (Figs. 1e and 1f). We further examined the infiltration of inflammatory cells and the expression of inflammatory cytokines in the liver. Immunohistochemical staining showed that MPO-positive inflammatory cell infiltration was significantly increased in the HS+I/R group (Figs. 1g and 1h). The qPCR results showed that the inflammatory cytokines interleukin-1β (*IL-1β*), monocyte chemoattractant protein-1 (*MCP-1*), and tumor necrosis factor-α (*TNF-α*) were significantly elevated in the HS+I/R group (Figs. 1j–1l).

Hypernatremia also aggravated hepatocyte apoptosis after IRI. Western blot analysis showed that the expression of pro-apoptotic proteins B-cell lymphoma 2 (BCL-2)-associated X protein (BAX) and cleaved caspase-3 (C-Caspase 3) was remarkably increased in the HS+I/R group, while the expression of anti-apoptotic protein BCL-2 was decreased (Fig. 1i). TUNEL staining showed that the number of apoptotic cells was significantly higher in the HS+I/R group than in the I/R group (Figs. 1m and 1n). To detect the levels of ROS in hepatic tissues, we performed DHE staining, which showed that the number of positive cells in the HS+I/R group was significantly higher than those in the other groups (Figs. 1o and 1p). The activity of GSH and SOD was significantly decreased in the HS+I/R group, whereas the MDA content was significantly elevated (Figs. 1q–1s). Thus, these results suggest that hypernatremia exacerbates hepatic IRI in Lewis rats.

3.2 Effect of HS on H/R injury in BRL-3A cells

To investigate the effect of HS on the H/R injury of hepatocytes, we constructed a cell model of HS+H/R by placing BRL-3A cells into 190 mmol/L HS DMEM for 24 h, followed by hypoxia for 6 h and reperfusion for additional 6 h (Fig. 2a). CCK-8 results showed that BRL-3A cells pretreated with HS before H/R decreased cell viability, which was most pronounced with HS pretreatment for 24 h (Fig. 2b). HS aggravated the apoptosis of hepatocytes after H/R; the flow cytometry results showed that the apoptosis rates of the cells were significantly increased after HS+H/R treatment (Figs. 2c and 2d). Western blot results showed that the expression of BAX and C-Caspase 3 was significantly increased in the HS+H/R group, while the expression of BCL-2 was markedly decreased (Fig. 2e). The fluorescence intensity of the ROS staining was elevated in the BRL-3A cells after H/R treatment, with the most pronounced elevation in the HS+H/R group (Figs. 2f and 2g). In conclusion, these results demonstrated that HS aggravates the damage caused by H/R in BRL-3A cells.

3.3 Amil's attenuation of hypernatremia-aggravated hepatic IRI in Lewis rats

To investigate the role of ENaC in hypernatremia-exacerbated IRI, we added Amil by intraperitoneal injection into rat models of I/R and HS+I/R. The serum results showed that the ALT, AST, and LDH levels of rats in the Amil+HS+I/R group were significantly lower than those in the HS+I/R group (Figs. 3a–3c).

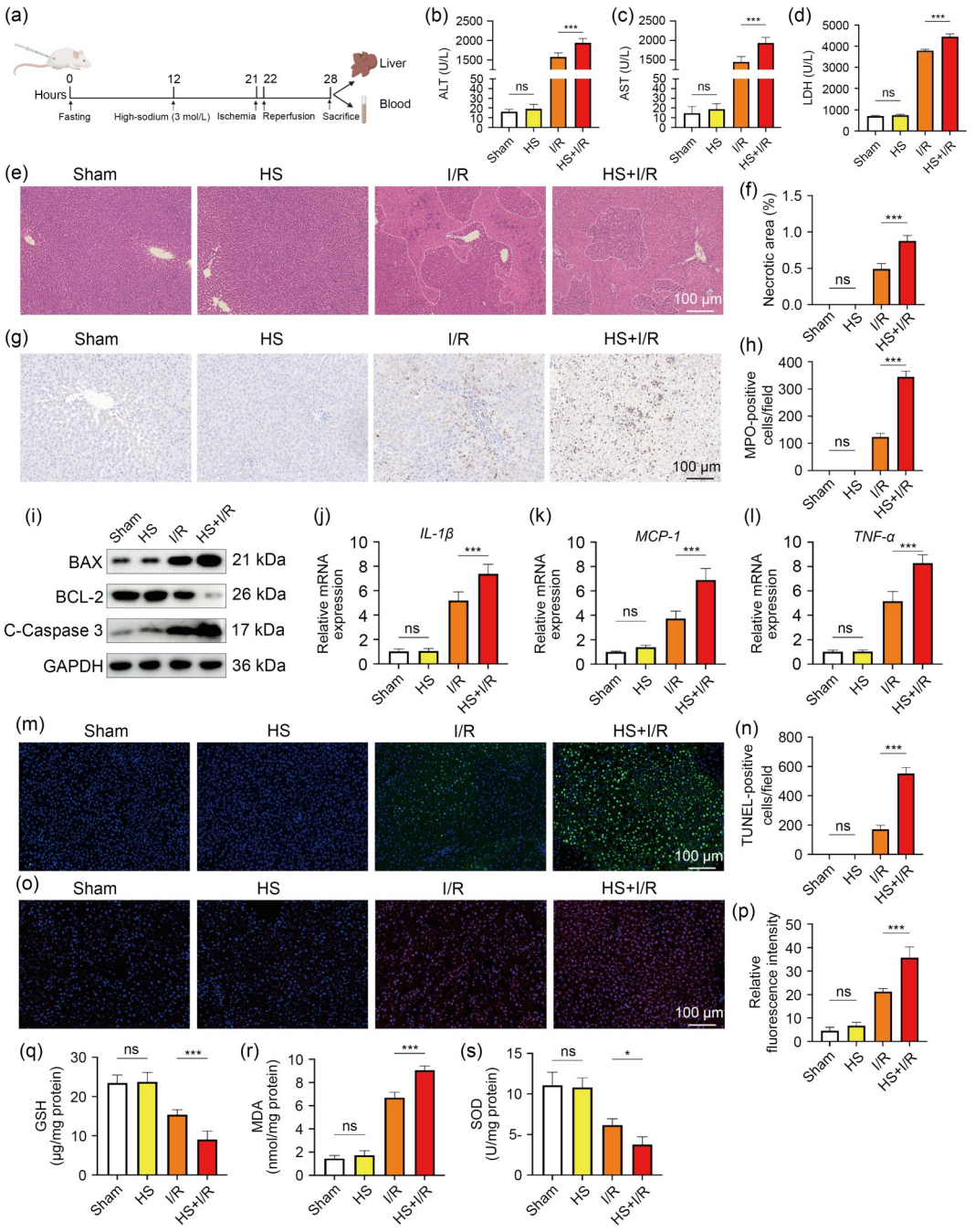

Fig. 1 Effect of hypernatremia on hepatic ischemia-reperfusion injury (IRI) in Lewis rats. (a) Flow chart for the construction of the ischemia-reperfusion (I/R) Lewis rat model of hypernatremia. (b–d) Serum alanine aminotransferase (ALT), aspartate aminotransferase (AST), and lactate dehydrogenase (LDH) levels in rats of the sham, HS (high-sodium), I/R, and HS+I/R groups (*n*=6). (e, f) Representative hepatic hematoxylin and eosin (H&E)-stained images and statistical chart showing necrotic areas (*n*=4). (g, h) Representative hepatic myeloperoxidase (MPO) immunohistochemical staining images and statistical chart (*n*=4). (i) Protein expression of B-cell lymphoma 2 (BCL-2)-associated X protein (BAX), BCL-2, and cleaved caspase-3 (C-Caspase 3) in hepatic tissues. (j–l) Messenger RNA (mRNA) levels of interleukin-1β (*IL-1β*), monocyte chemoattractant protein-1 (*MCP-1*), and tumor necrosis factor-α (*TNF-α*) in hepatic tissues. (m, n) Representative hepatic terminal deoxynucleotidyl transferase dUTP nick-end labeling (TUNEL) staining images and statistical chart (*n*=4). (o, p) Representative hepatic dihydroethidium (DHE) staining images and statistical chart (*n*=4). (q–s) Hepatic glutathione (GSH) activity, malondialdehyde (MDA) content, and superoxide dismutase (SOD) activity in the sham, HS, I/R, and HS+I/R groups (*n*=6). GAPDH: glyceraldehyde 3-phosphate dehydrogenase. Data are expressed as mean± standard deviation (SD). ns, not significant; * *P*<0.05, * *P*<0.001.**

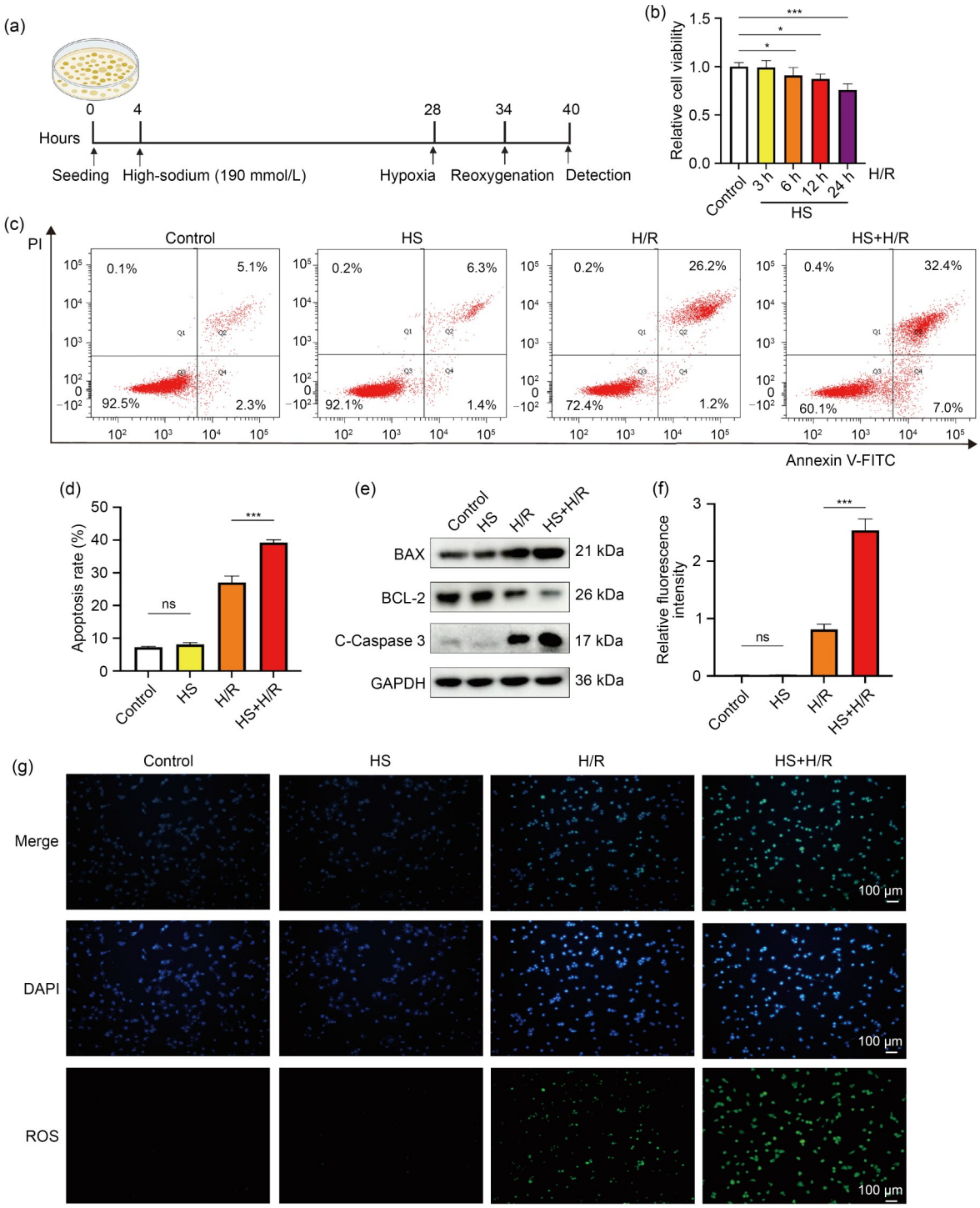

Fig. 2 Effect of high-sodium (HS) on hypoxia-reoxygenation (H/R) injury in BRL-3A cells. (a) Flow chart for the construction of the BRL-3A cell model of HS+H/R. (b) Viability of BRL-3A cells treated with 190 mmol/L HS DMEM for 3, 6, 12, and 24 h followed by H/R treatment was detected using cell-counting kit-8 (CCK-8) assays. (c, d) Cell apoptosis rates were determined by flow cytometry and statistical chart (n=4). (e, f) Protein expression of BAX, BCL-2, and C-Caspase 3 in BRL-3A cells and statistical chart (n=4). (g) Representative reactive oxygen species (ROS), 4',6-diamidino-2'-phenylindol (DAPI), and merged staining images of BRL-3A cells in the control, HS, H/R, and HS+H/R groups. BAX: B-cell lymphoma 2 (BCL-2)-associated X protein; C-Caspase 3: cleaved caspase-3; DMEM: Dulbecco's modified Eagle's medium; GAPDH: glyceraldehyde 3-phosphate dehydrogenase; FITC: fluorescein isothiocyanate; PI: propidium iodide. Data are expressed as mean±standard deviation (SD). ns, not significant; * P<0.05, *** P<0.001.

The area of hepatic necrosis in the Amil+HS+I/R group was significantly smaller than that in the HS+I/R group, as shown in H&E-stained images (Figs. 3d and 3e). Amil alleviated hypernatremia-induced hepatic IRI, while also reducing hepatic inflammation. Immunohistochemical staining showed that MPO-positive inflammatory cell infiltration was significantly reduced in the Amil+HS+I/R group compared to that in the HS+I/R group (Figs. 3f and 3g). The messenger RNA (mRNA) levels of *IL-1β*, *MCP-1*, and *TNF-α* in the hepatic tissues of the Amil+HS+I/R group were significantly lower than those of the HS+I/R group (Figs. 3i–3k).

To determine the effect of Amil on hepatocyte apoptosis in hypernatremia liver I/R, we performed a western blot experiment. The results showed that Amil treatment decreased the expression of BAX, C-Caspase 3, and NLRP3 in the hepatic tissues, while increasing the expression of BCL-2 (Fig. 3h). TUNEL staining confirmed that the number of positive cells was decreased in the Amil+HS+I/R group compared to the HS+I/R group (Figs. 3o and 3p). After the addition of Amil, the activity of GSH and SOD was increased in the hepatic tissues, while the MDA content was significantly decreased (Figs. 3l–3n); correspondingly, the fluorescence intensity of DHE staining was significantly decreased in the Amil+HS+I/R group compared to that in the HS+I/R group (Figs. 3q and 3r). Therefore, Amil could attenuate hypernatremia-exacerbated hepatic IRI in Lewis rats.

3.4 Amil's attenuation of HS-exacerbated H/R injury in BRL-3A cells

The CCK-8 results showed that, in the BRL-3A cells of the Amil+HS+H/R group, cell viability was significantly improved at an Amil concentration of 10 μmol/L. Thus, we used 10 μmol/L as the concentration for the Amil cell experiments (Fig. 4a). Amil reduced hepatocyte apoptosis after H/R in the HS state. Flow cytometry results showed that the apoptosis rate of cells in the Amil+HS+H/R group was significantly lower than that in the HS+H/R group (Figs. 4b and 4d). Western blot analysis showed that the expression of BAX, C-Caspase 3, and NLRP3 was decreased in the Amil+HS+H/R group compared to the HS+H/R group. In contrast, BCL-2 expression was elevated (Fig. 4c). The fluorescence intensity of ROS staining was significantly lower in the Amil+HS+H/R group than in the HS+H/R group (Figs. 4e and 4f). In conclusion, Amil could attenuate HS-exacerbated H/R injury in BRL-3A cells.

3.5 SN-6's attenuation of hypernatremia-aggravated hepatic IRI in Lewis rats

To study the role of NCX in hypernatremia-exacerbated hepatic IRI, we injected SN-6 into rats by intraperitoneal injection. The serum levels of ALT, AST, and LDH were significantly lower in the SN-6+HS+I/R group than in the HS+I/R group (Figs. 5a–5c). The H&E-stained images showed that the area of hepatic necrosis was significantly reduced in the SN-6+HS+I/R group compared to the HS+I/R group (Figs. 5d and 5e). Immunohistochemical staining showed that MPO-positive inflammatory cell infiltration was significantly lower in the SN-6+HS+I/R group than in the HS+I/R group (Figs. 5f and 5g). Meanwhile, qPCR results showed that the mRNA levels of *IL-1β*, *MCP-1*, and *TNF-α* were significantly lower in the SN-6+HS+I/R group than in the HS+I/R group (Figs. 5i–5k).

The results of the western blot showed that SN-6 treatment decreased the expression of BAX, C-Caspase 3, and NLRP3 and promoted the expression of BCL-2 (Fig. 5h). TUNEL staining found that SN-6 could reduce the number of TUNEL-positive cells in the hepatic tissues (Figs. 5o and 5p). The activity of GSH and SOD was higher in the SN-6+HS+I/R group than in the HS+I/R group (Figs. 5l and 5n). The MDA content was reversed (Fig. 5m), while the fluorescence intensity of DHE staining was lower in the SN-6+HS+I/R group than in the HS+I/R group (Figs. 5q and 5r). In summary, SN-6 could alleviate hepatic IRI exacerbated by hypernatremia.

3.6 SN-6's attenuation of HS-aggravated H/R injury in BRL-3A cells

We first explored the optimal experimental concentration of SN-6 using the CCK-8 experiment. The results showed that the cell viability of HS+H/R BRL-3A cells was significantly improved when the concentration of SN-6 reached 10 μmol/L; therefore, we selected 10 μmol/L as the concentration for SN-6 cell experiments (Fig. 6a). Next, the effect of SN-6 on hepatocyte apoptosis was further detected; western blot analysis found that the addition of SN-6 significantly decreased the expression of BAX, C-Caspase 3, and NLRP3. In contrast, the expression of BCL-2 was

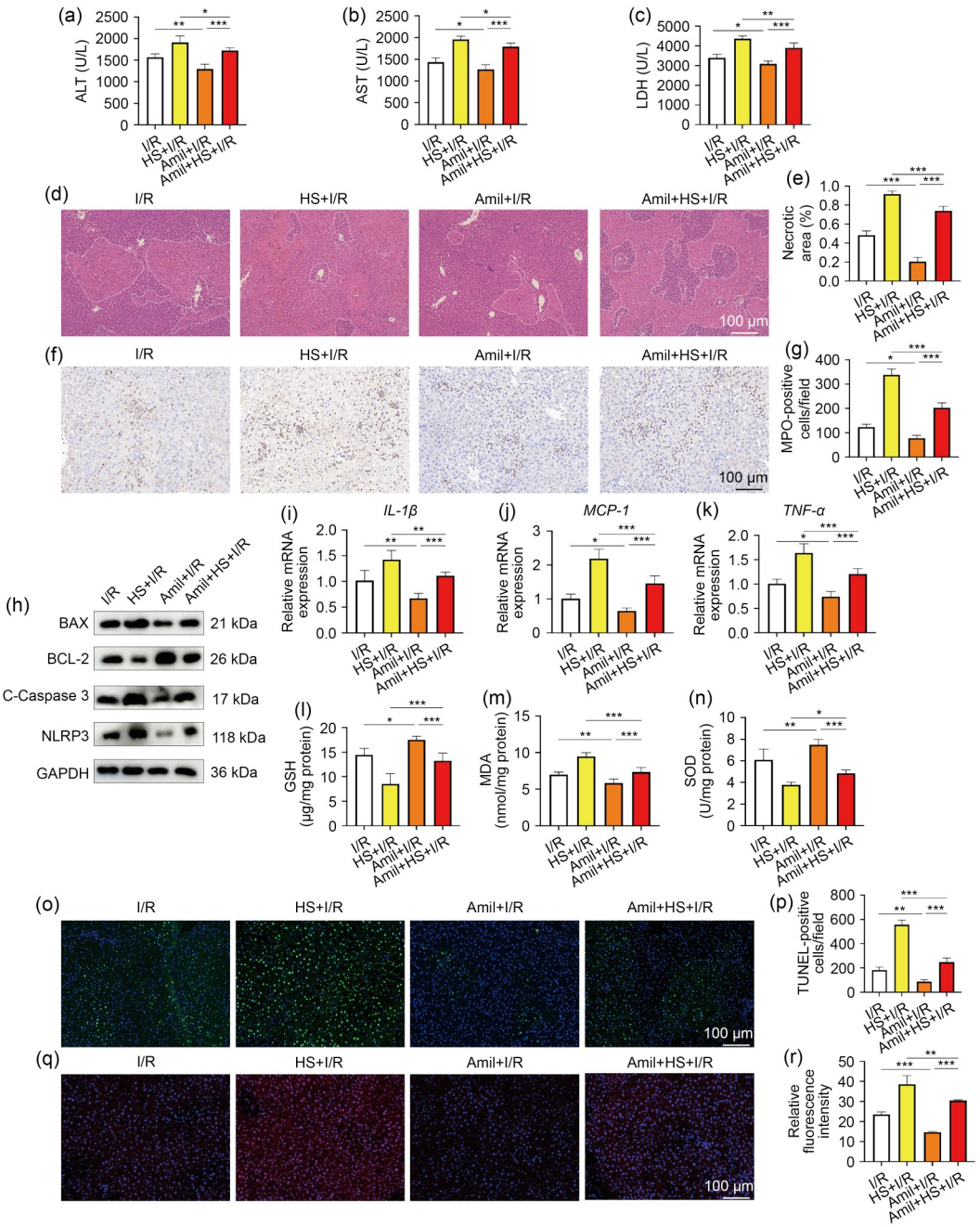

Fig. 3 Amiloride (Amil)'s attenuation of hypernatremia-aggravated hepatic ischemia-reperfusion injury (IRI) in Lewis rats. (a–c) Serum alanine aminotransferase (ALT), aspartate aminotransferase (AST), and lactate dehydrogenase (LDH) levels in rats of the I/R, HS+I/R, Amil+I/R, and Amil+HS+I/R groups (*n*=6). (d, e) Representative hepatic hematoxylin and eosin (H&E)-stained images and statistical chart showing necrotic areas (*n*=4). (f, g) Representative hepatic MPO immunohistochemical staining images and statistical chart (*n*=4). (h) The protein expression of BAX, BCL-2, C-Caspase 3, and NOD-like receptor family, pyrin domain-containing 3 (NLRP3) in hepatic tissues. (i–k) The mRNA levels of *IL-1β*, *MCP-1*, and *TNF-α* in hepatic tissues. (l–n) Hepatic glutathione (GSH) activity, malondialdehyde (MDA) content, and superoxide dismutase (SOD) activity in rats of the I/R, HS+I/R, Amil+I/R, and Amil+HS+I/R groups (*n*=6). (o, p) Representative hepatic terminal deoxynucleotidyl transferase dUTP nick-end labeling (TUNEL) staining images and statistical chart (*n*=4). (q, r) Representative hepatic dihydroethidium (DHE) staining images and statistical chart in rats (*n*=4). I/R: ischemia-reperfusion; HS: high-sodium; MPO: myeloperoxidase; BAX: B-cell lymphoma 2 (BCL-2)-associated X protein; C-Caspase 3: cleaved caspase-3; GAPDH: glyceraldehyde 3-phosphate dehydrogenase; mRNA: messenger RNA; *IL-1β*: interleukin-1β; *MCP-1*: monocyte chemoattractant protein-1; *TNF-α*: tumor necrosis factor-α. Data are expressed as mean±standard deviation (SD). * *P*<0.05, ** *P*<0.01, *** *P*<0.001.

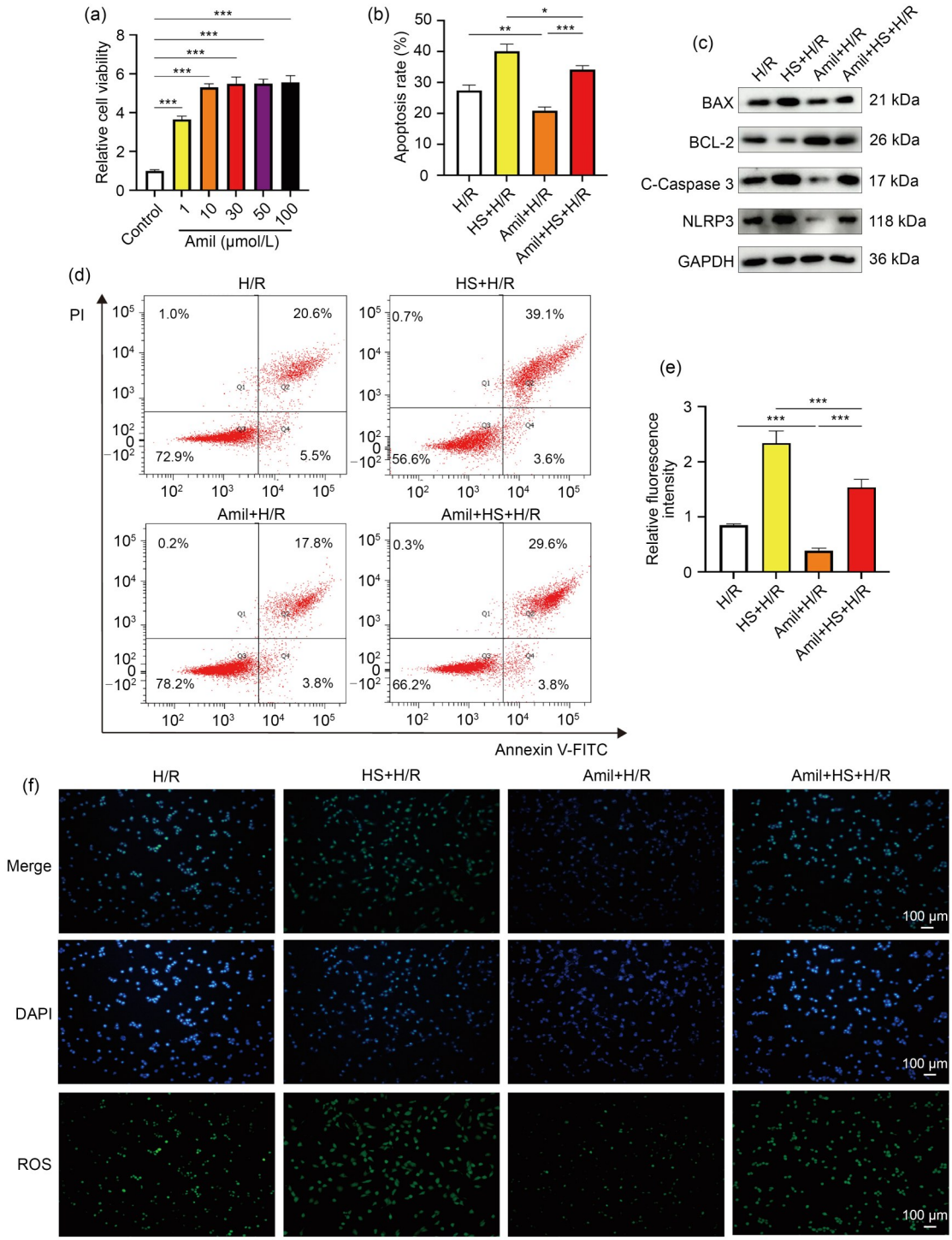

Fig. 4 Amil's attenuation of HS-aggravated H/R injury in BRL-3A cells. (a) Viability of BRL-3A cells treated with different concentrations of Amil under the HS+H/R condition was detected using CCK-8 assays. (b, d) Statistical chart (*n*=4) and cell apoptosis rates were determined by flow cytometry. (c) Protein expression of BAX, BCL-2, C-Caspase 3, and NLRP3 in BRL-3A cells. (e, f) Statistical chart (*n*=4) and representative ROS, DAPI, and merged staining images of BRL-3A cells in the H/R, HS+H/R, Amil+H/R, and Amil+HS+H/R groups. HS: high-sodium; H/R: hypoxia-reoxygenation; CCK-8: cell-counting kit-8; BAX: B-cell lymphoma 2 (BCL-2)-associated X protein; C-Caspase 3: cleaved caspase-3; NLRP3: NOD-like receptor family, pyrin domain-containing 3; GAPDH: glyceraldehyde 3-phosphate dehydrogenase; DAPI: 4',6-diamidino-2'-phenylindol; ROS: reactive oxygen species. Data are expressed as mean±standard deviation (SD). * *P*<0.05, ** *P*<0.01, *** *P*<0.001.

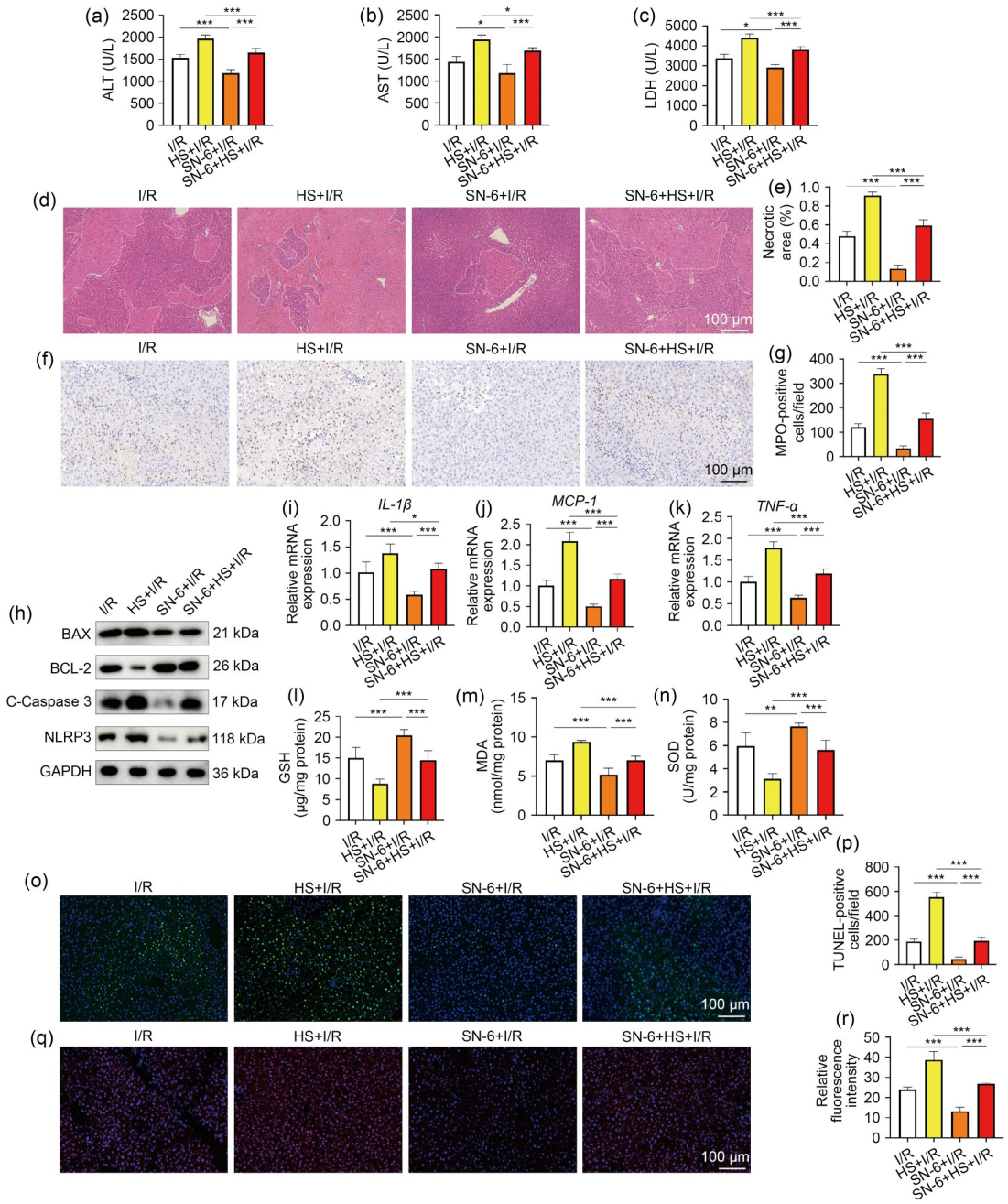

Fig. 5 SN-6's attenuation of hypernatremia-aggravated hepatic ischemia-reperfusion injury (IRI) in Lewis rats. (a–c) Serum alanine aminotransferase (ALT), aspartate aminotransferase (AST), and lactate dehydrogenase (LDH) levels in rats of the ischemia-reperfusion (I/R), high-sodium (HS)+I/R, SN-6+I/R, and SN-6+HS+I/R groups (*n*=6). (d, e) Representative hepatic hematoxylin and eosin (H&E)-stained images and statistical chart showing necrotic areas (*n*=4). (f, g) Representative hepatic myeloperoxidase (MPO) immunohistochemical staining images and statistical chart (*n*=4). (h) Protein expression of B-cell lymphoma 2 (BCL-2)-associated X protein (BAX), BCL-2, cleaved caspase-3 (C-Caspase 3), and NOD-like receptor family, pyrin domain-containing 3 (NLRP3) in hepatic tissues. (i–k) Messenger RNA (mRNA) levels of interleukin-1β (*IL-1β*), monocyte chemoattractant protein-1 (*MCP-1*), and tumor necrosis factor-α (*TNF-α*) in hepatic tissues. (l–n) Hepatic glutathione (GSH) activity, malondialdehyde (MDA) content, and superoxide dismutase (SOD) activity in rats of the I/R, HS+I/R, SN-6+I/R, and SN-6+HS+I/R groups (*n*=6). (o, p) Representative hepatic terminal deoxynucleotidyl transferase dUTP nick-end labeling (TUNEL) staining images and statistical chart (*n*=4). (q, r) Representative hepatic dihydroethidium (DHE) staining images and statistical chart in rats (*n*=4). GAPDH: glyceraldehyde 3-phosphate dehydrogenase. Data are expressed as mean±standard deviation (SD). * *P*<0.05, ** *P*<0.01, * *P*<0.001.**

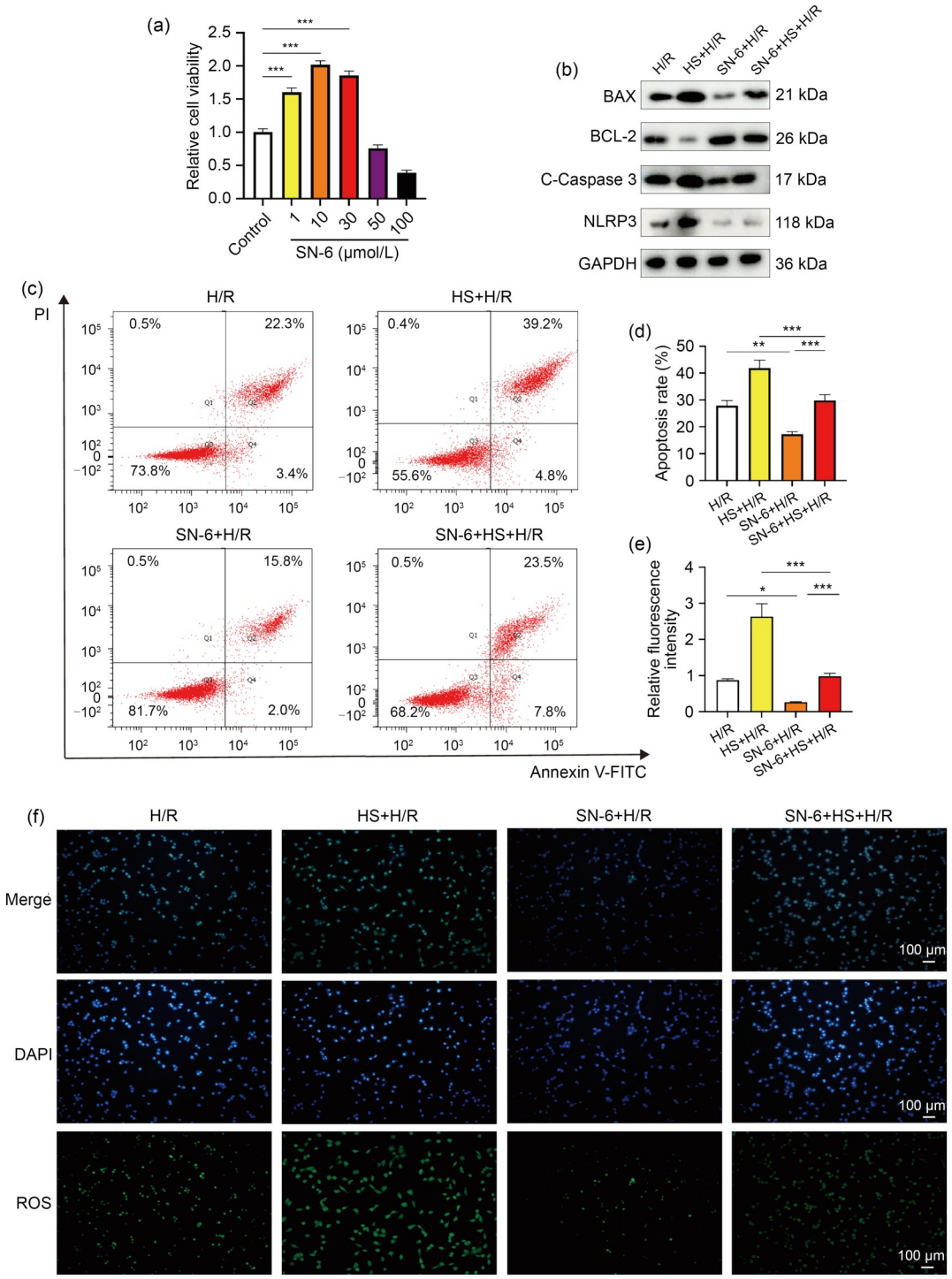

Fig. 6 SN-6's attenuation of HS-aggravated H/R injury in BRL-3A cells. (a) Viability of BRL-3A cells treated with different concentrations of SN-6 under the HS+H/R condition was detected using CCK-8 assays. (b) Protein expression of BAX, BCL-2, C-Caspase 3, and NLRP3 in BRL-3A cells. (c, d) Cell apoptosis rates were determined by flow cytometry and statistical chart (*n*=4). (e, f) Representative ROS, DAPI, and merged staining images of BRL-3A cells in the H/R, HS+H/R, SN-6+I/R, and SN-6+HS+I/R groups and statistical chart (*n*=4). HS: high-sodium; H/R: hypoxia-reoxygenation; CCK-8: cell-counting kit-8; BAX: B-cell lymphoma 2 (BCL-2)-associated X protein; C-Caspase 3: cleaved caspase-3; NLRP3: NOD-like receptor family, pyrin domain-containing 3; GAPDH: glyceraldehyde 3-phosphate dehydrogenase; DAPI: 4',6-diamidino-2'-phenylindol; ROS: reactive oxygen species. Data are expressed as mean±standard deviation (SD). * *P*< 0.05, ** *P*<0.01, *** *P*<0.001.

increased in the SN-6+HS+H/R group compared to the HS+H/R group (Fig. 6b). Flow cytometry results showed that the apoptosis rates were significantly decreased in the SN-6+HS+H/R group compared to the HS+H/R group (Figs. 6c and 6d). The fluorescence intensity of ROS staining in the SN-6+HS+H/R group was significantly lower than that that in the HS+H/R group (Figs. 6e and 6f). In conclusion, SN-6 could attenuate HS-enhanced H/R injury in BRL-3A cells.

4 Discussion

Donors for LT are mainly deceased donors, categorized as donors after brain death (DBD) or donors after circulatory death (DCD). Due to excessive infusion of sodium-containing fluids, increased aldosterone, and renal dysfunction, donors often suffer from hypernatremia (Ilardi, 2022; Bernal et al., 2023). Elevated donor serum sodium concentrations have been widely reported to adversely affect LT, and the results of a systematic study that included 25 study cohorts and 19 389 LT recipients suggested that donor hypernatremia is associated with poor liver function in the early postoperative period (Basmaji et al., 2020). Livers from donors with serum sodium concentrations of >155 mmol/L are considered extended-criteria donor livers with a potential risk of poor prognosis (Basmaji et al., 2020; McDonald et al., 2021). However, the molecular mechanisms underlying this clinical phenomenon remain unreported. In our study, we found that hypernatremia aggravated IRI in Lewis rat livers, and HS also aggravated H/R injury in BRL-3A cells, which was associated with ENaC and NCX. Their specific inhibitors could be applied to reduce the negative effects of hypernatremia on hepatic I/R (Fig. 7).

It has been widely reported that I/R increases hepatic inflammation and injury (Guo et al., 2020; Ding et al., 2022), and we found that hepatic IRI was further exacerbated in hypernatremia rats. We constructed the I/R model of Lewis rats with hypernatremia; the serum levels of ALT, AST, and LDH, and the area of hepatic ischemic necrosis were all significantly higher in the HS+I/R group than in the I/R group. The inflammatory cytokines and ROS in the livers were

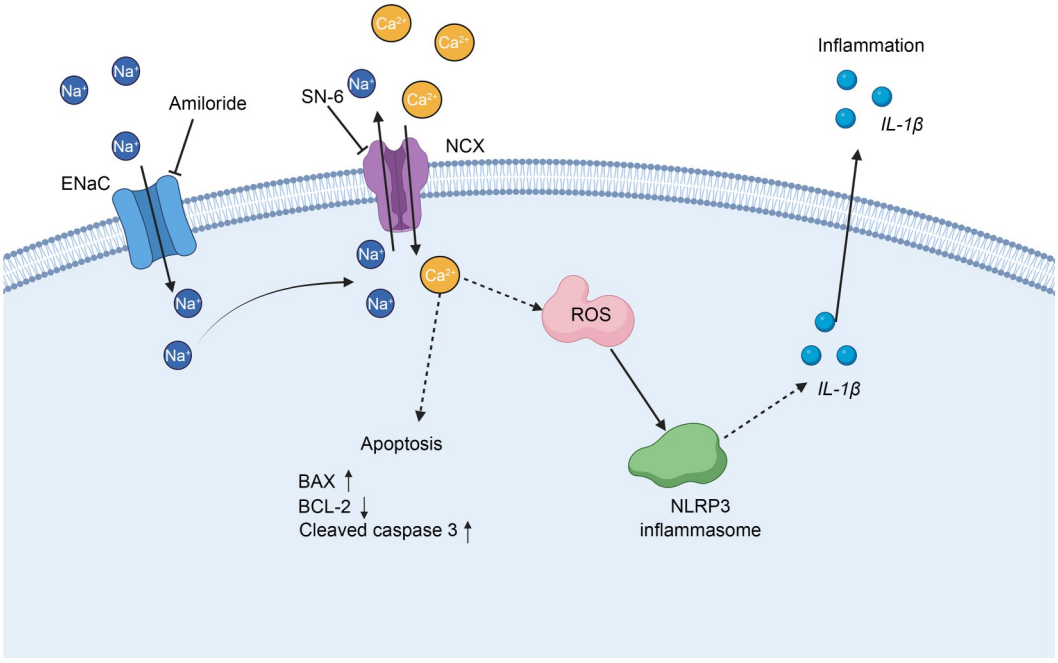

Fig. 7 Schematic diagram of the mechanism by which hypernatremia aggravates hepatic ischemia-reperfusion injury (IRI). Elevated extracellular Na^+ leads to the increase of the entry of Na^+ into the cell via epithelial sodium channel (ENaC). Increased intracellular Na^+ promotes the exchange of intracellular Na^+ with extracellular Ca^{2+} via Na^+/Ca^{2+} exchanger (NCX). Intracellular Ca^{2+} overload leads to increased production of reactive oxygen species (ROS) and NOD-like receptor family, pyrin domain-containing 3 (NLRP3), which ultimately enhances cellular apoptosis and inflammation. The inhibitors of ENaC and NCX, Amil and SN-6, respectively, can reduce hypernatremia-aggravated hepatic IRI. BAX: B-cell lymphoma 2 (BCL-2)-associated X protein; *IL-1β*: interleukin-1β.

increased in the HS+I/R group, as evidenced by increased levels of *IL-1β*, *MCP-1*, and *TNF-α*, elevated content of MDA, and decreased activity of GSH and SOD (Chen et al., 2022; Han et al., 2022). Similar results were found in the BRL-3A cells, where the fluorescence intensity of the ROS staining of the cells in the HS+H/R group was significantly increased, and flow cytometry showed an increase in cellular apoptosis. The western blot analysis showed increased expression of BAX and C-Caspase 3 in both the HS+I/R group of rats and the HS+H/R group of cells. Exacerbation of IRI by hypernatremia has been reported in the heart (Castaldo et al., 2017) and kidney (Matsumoto et al., 2022). The molecular mechanism of exacerbated IRI by hypernatremia is related to the activation of ENaC (Matsumoto et al., 2022) and NCX (Castaldo et al., 2017), which leads to intracellular calcium overload. Therefore, we applied specific inhibitors of ENaC and NCX to validate their roles in hepatic IRI aggravated by hypernatremia.

ENaC is a type of sodium channel that is usually composed of α, β, and γ subunits. ENaC primarily maintains cellular sodium homeostasis, and it has been reported to be closely associated with ROS production in cystic fibrosis and cardiovascular sclerosis (Pitzer et al., 2022; Chen et al., 2023). ENaC-mediated extracellular Na^+ influx elevates intracellular Na^+, and increased exchange of Na^+ and Ca^{2+} leads to intracellular Ca^{2+} overload, which activates Ca^{2+}-related signaling pathways, leading to increased ROS production and pro-inflammatory cytokine release and facilitating cellular apoptosis (Dizin et al., 2021; Pitzer et al., 2022). αENaC knockout attenuated renal IRI in mice, and the application of 1 μmol/L Amil in human microvascular endothelial cells (HMEC-1) promoted the activation of endothelial nitric oxide synthase (eNOS) (Tarjus et al., 2019). Knockout of γENaC could also increase eNOS in the kidney (Mutchler et al., 2021). Na^+ was enriched, and NCX activity was increased in neuronal cells after global cerebral ischemia, and neuronal cell death could be alleviated by intraperitoneal injection of Amil in a mouse model (Kang et al., 2020). In our study, we found that the application of Amil reduced hepatic inflammation and cellular apoptosis. Hepatic ROS production was decreased in the Amil+HS+I/R and Amil+HS+H/R groups. Alleviated hepatic inflammation was evidenced by reduced MPO-positive cellular infiltration and decreased levels of *IL-1β*, *MCP-1*, and *TNF-α*. These results demonstrated that inhibition of ENaC attenuated the effects of hypernatremia on hepatic IRI.

NCX mediates the cellular exchange of Na^+ and Ca^{2+}, and NCX-1 is an isoform of NCX (Xue et al., 2023). Transient ischemia led to increased Na^+ concentration in astrocytes, followed by increased NCX activity, promoting Na^+ efflux (Gerkau et al., 2018). The elevation of the Na^+ concentration in the perfusate from 145 to 155 mmol/L aggravated cardiac IRI, and the adverse effects caused by HS could be alleviated by the application of an inhibitor of NCX (King et al., 2020). After I/R of cardiomyocytes, NCX-1 expression was increased, and myocardial IRI was reduced after application of SN-6 (Hu et al., 2019; Li et al., 2019; Shi et al., 2023). Activation of NCX caused intracellular Ca^{2+} accumulation, which in turn led to a rise in ROS production and promoted the production of pro-inflammatory cytokines and apoptosis (Castaldo et al., 2017). After myocardial I/R, Na^+ and Ca^{2+} overload in cardiomyocytes led to NLRP3 activation and increased IL-1β release. Dapagliflozin inhibited the activity of NCX on cardiomyocytes, reduced intracellular Ca^{2+}, and decreased the inflammation and apoptosis of cardiomyocytes (Yu et al., 2021). NCX expression was increased after myocardial infarction, and rosmarinic acid prevented myocardial hypertrophy and cardiac dysfunction by inhibiting NCX (Javidanpour et al., 2018). After the application of SN-6, our study found that cellular ROS production and the number of MPO-positive cells were reduced in the SN-6+HS+H/R group. BAX and C-Caspase 3 expression levels were decreased, BCL-2 expression level was increased both in the SN-6+HS+I/R and SN-6+HS+H/R groups, and cellular apoptosis was reduced as shown by flow cytometry and TUNEL fluorescence intensity, demonstrating that SN-6 could improve HS-induced IRI.

In this study, we applied original animal and cellular models of HS. Our experiments verified that a stable rat model with 190 mmol/L serum sodium concentration could be established by applying a 3 mol/L NaCl solution administered via tail vein infusion. During the induction period, 0.7 mL of 3 mol/L NaCl solution per 100 g BW was first pumped through the tail vein over 5 min. Then, 0.7 mL/h of 3 mol/L NaCl solution was continuously pumped during the ascending period, and the serum sodium concentration

could typically reach 190 mmol/L after 3 h. Finally, the pumping rate during the maintenance period was adjusted to 0.2 mL/h. For the HS cell model, BRL-3A cells were cultured with 190 mmol/L HS DMEM for 24 h before H/R. These novel animal and cellular models simulate the process of LT from hypernatremia donor livers and provide tools to study the role of hypernatremia in hepatic IRI.

There are some shortcomings in our study: we did not apply gene-edited cells or animals for the study, and in addition, the rat model of hypernatremia was relatively transient because it was difficult to establish a long-term stable rat model with serum sodium concentrations up to 190 mmol/L. Therefore, it would be meaningful to apply the gene knockout or overexpression models of ENaC and NCX further for in vivo and in vitro experiments. As liver sinusoidal endothelial cells (LSECs) and Kupffer cells play an important role in hepatic IRI, we speculate that the concentrations of Na^+ and Ca^{2+} in these cells will also increase under HS conditions, and that calcium overload leads to the activation of downstream inflammation and apoptosis pathways. Therefore, to study the mechanism by which hypernatremia aggravates hepatic IRI, it will be valuable to further isolate primary LSECs and Kupffer cells for in vitro experiments.

In summary, our study demonstrated that the exacerbation of hepatic IRI by hypernatremia is related to ENaC and NCX, and that the application of the specific inhibitors Amil and SN-6 could attenuate hepatic IRI exacerbated by hypernatremia. Our conclusions suggest a new therapeutic option for hypernatremia donors and contribute to improving the utilization rate of hypernatremia donor livers.

Data availability statement

All relevant data are included in the article and supplementary materials.

Acknowledgments

This work was supported by the Funding for Scientific Research and Innovation Team of The First Affiliated Hospital of Zhengzhou University (No. ZYCXTD2023007), China.

Author contributions

Wenzhi GUO and Yabin CHEN designed the experiments. Yabin CHEN, Hao LI, and Peihao WEN performed the experiments. Jiakai ZHANG and Zhihui WANG analyzed the data and wrote the manuscript. Shengli CAO collected the data and edited the grammar. All authors have read and approved the final manuscript, and therefore, have full access to all the data in the study and take responsibility for the integrity and security of the data.

Compliance with ethics guidelines

Yabin CHEN, Hao LI, Peihao WEN, Jiakai ZHANG, Zhihui WANG, Shengli CAO, and Wenzhi GUO declare that they have no conflicts of interest.

This study was approved by the Clinical Research Ethics Committee of the First Affiliated Hospital of Zhengzhou University (Ref: 2023-KY-0006). All rats were cared in accordance with the Guide for the Care and Use of Laboratory Animals.

References

Basmaji J, Hornby L, Rochwerg B, et al., 2020. Impact of donor sodium levels on clinical outcomes in liver transplant recipients: a systematic review. *Eur J Gastroenterol Hepatol*, 32(12):1489-1496. https://doi.org/10.1097/MEG.0000000000001776

Bastos-Neves D, Salvalaggio PRO, Almeida MD, 2019. Risk factors, surgical complications and graft survival in liver transplant recipients with early allograft dysfunction. *Hepatobiliary Pancreat Dis Int*, 18(5):423-429. https://doi.org/10.1016/j.hbpd.2019.02.005

Bernal A, Zafra MA, Simón MJ, et al., 2023. Sodium homeostasis, a balance necessary for life. *Nutrients*, 15(2):395. https://doi.org/10.3390/nu15020395

Castaldo P, Macri ML, Lariccia V, et al., 2017. Na^+/Ca^{2+} exchanger 1 inhibition abolishes ischemic tolerance induced by ischemic preconditioning in different cardiac models. *Eur J Pharmacol*, 794:246-256. https://doi.org/10.1016/j.ejphar.2016.11.045

Ceresa CDL, Nasralla D, Pollok JM, et al., 2022. Machine perfusion of the liver: applications in transplantation and beyond. *Nat Rev Gastroenterol Hepatol*, 19(3):199-209. https://doi.org/10.1038/s41575-021-00557-8

Chen QB, Li Q, Liang YQ, et al., 2022. Natural exosome-like nanovesicles from edible tea flowers suppress metastatic breast cancer *via* ROS generation and microbiota modulation. *Acta Pharm Sin B*, 12(2):907-923. https://doi.org/10.1016/j.apsb.2021.08.016

Chen SY, Zhang HP, Li J, et al., 2021. Tripartite motif-containing 27 attenuates liver ischemia/reperfusion injury by suppressing transforming growth factor β-activated kinase 1 (TAK1) by TAK1 binding protein 2/3 degradation. *Hepatology*, 73(2):738-758. https://doi.org/10.1002/hep.31295

Chen YB, Yu X, Yan ZP, et al., 2023. Role of epithelial sodium channel-related inflammation in human diseases. *Front Immunol*, 14:1178410. https://doi.org/10.3389/fimmu.2023.1178410

Dar WA, Sullivan E, Bynon JS, et al., 2019. Ischaemia reperfusion injury in liver transplantation: cellular and molecular mechanisms. *Liver Int*, 39(5):788-801.

https://doi.org/10.1111/liv.14091

Ding MJ, Fang HR, Zhang JK, et al., 2022. E3 ubiquitin ligase ring finger protein 5 protects against hepatic ischemia reperfusion injury by mediating phosphoglycerate mutase family member 5 ubiquitination. *Hepatology*, 76(1): 94-111.
https://doi.org/10.1002/hep.32226

Dizin E, Olivier V, Roth I, et al., 2021. Activation of the hypoxia-inducible factor pathway inhibits epithelial sodium channel-mediated sodium transport in collecting duct principal cells. *J Am Soc Nephrol*, 32(12):3130-3145.
https://doi.org/10.1681/ASN.2021010046

Frindt G, Yang L, Bamberg K, et al., 2018. Na restriction activates epithelial Na channels in rat kidney through two mechanisms and decreases distal Na^+ delivery. *J Physiol*, 596(16):3585-3602.
https://doi.org/10.1113/JP275988

Gerkau NJ, Rakers C, Durry S, et al., 2018. Reverse NCX attenuates cellular sodium loading in metabolically compromised cortex. *Cereb Cortex*, 28(12):4264-4280.
https://doi.org/10.1093/cercor/bhx280

Guo WZ, Fang HB, Cao SL, et al., 2020. Six-transmembrane epithelial antigen of the prostate 3 deficiency in hepatocytes protects the liver against ischemia-reperfusion injury by suppressing transforming growth factor-β-activated kinase 1. *Hepatology*, 71(3):1037-1054.
https://doi.org/10.1002/hep.30882

Guo ZY, Zhao Q, Jia ZH, et al., 2023. A randomized-controlled trial of ischemia-free liver transplantation for end-stage liver disease. *J Hepatol*, 79(2):394-402.
https://doi.org/10.1016/j.jhep.2023.04.010

Han MJ, Lin J, Yang Y, et al., 2022. Xinshuaining preparation protects H9c2 cells from H_2O_2-induced oxidative damage through the PI3K/AKt/Nrf-2 signaling pathway. *Clin Exp Hypertens*, 45(1):1-9.
https://doi.org/10.1080/10641963.2022.2131806

Hu HJ, Wang SS, Wang YX, et al., 2019. Blockade of the forward Na^+/Ca^{2+} exchanger suppresses the growth of glioblastoma cells through Ca^{2+}-mediated cell death. *Br J Pharmacol*, 176(15):2691-2707.
https://doi.org/10.1111/bph.14692

Ilardi A, 2022. Diagnostic and therapeutic approach to hypernatremia. *Diagnosis (Berl)*, 9(4):403-410.
https://doi.org/10.1515/dx-2022-0034

Javidanpour S, Dianat M, Badavi M, et al., 2018. The inhibitory effect of rosmarinic acid on overexpression of NCX1 and stretch-induced arrhythmias after acute myocardial infarction in rats. *Biomed Pharmacother*, 102:884-893.
https://doi.org/10.1016/j.biopha.2018.03.103

Kaltenmeier C, Yazdani HO, Handu S, et al., 2022. The role of neutrophils as a driver in hepatic ischemia-reperfusion injury and cancer growth. *Front Immunol*, 13:887565.
https://doi.org/10.3389/fimmu.2022.887565

Kang BS, Choi BY, Kho AR, et al., 2020. An inhibitor of the sodium-hydrogen exchanger-1 (NHE-1), amiloride, reduced zinc accumulation and hippocampal neuronal death after ischemia. *Int J Mol Sci*, 21(12):4232.
https://doi.org/10.3390/ijms21124232

King DR, Padget RL, Perry J, et al., 2020. Elevated perfusate [Na^+] increases contractile dysfunction during ischemia and reperfusion. *Sci Rep*, 10:17289.
https://doi.org/10.1038/s41598-020-74069-x

Li JY, Yu DS, He CH, et al., 2023. KLF6 alleviates hepatic ischemia-reperfusion injury by inhibiting autophagy. *Cell Death Dis*, 14(7):393.
https://doi.org/10.1038/s41419-023-05872-3

Li Y, Quan X, Li XL, et al., 2019. Kdm6A protects against hypoxia-induced cardiomyocyte apoptosis via H3K27me3 demethylation of Ncx gene. *J Cardiovasc Transl Res*, 12(5):488-495.
https://doi.org/10.1007/s12265-019-09882-5

Lin YM, Huang HT, Chen LF, et al., 2023. Assessing donor liver quality and restoring graft function in the era of extended criteria donors. *J Clin Transl Hepatol*, 11(1):219-230.
https://doi.org/10.14218/JCTH.2022.00194

Lucas-Ruiz F, Mateo SV, Jover-Aguilar M, et al., 2023. Danger signals released during cold ischemia storage activate NLRP3 inflammasome in myeloid cells and influence early allograft function in liver transplantation. *EBioMedicine*, 87:104419.
https://doi.org/10.1016/j.ebiom.2022.104419

Matsumoto T, Doi S, Nakashima A, et al., 2022. Upregulation of mineralocorticoid receptor contributes to development of salt-sensitive hypertension after ischemia-reperfusion injury in rats. *Int J Mol Sci*, 23(14):7831.
https://doi.org/10.3390/ijms23147831

McDonald MF, Barrett SC, Malik TH, et al., 2021. Elevated serum sodium in recipients of liver transplantation has a substantial impact on outcomes. *Transpl Int*, 34(10):1971-1983.
https://doi.org/10.1111/tri.13968

Mutchler SM, Hasan M, Kohan DE, et al., 2021. Deletion of the gamma subunit of ENaC in endothelial cells does not protect against renal ischemia reperfusion injury. *Int J Mol Sci*, 22(20):10914.
https://doi.org/10.3390/ijms222010914

N'Gouemo P, 2013. Probing the role of the sodium/calcium exchanger in pentylenetetrazole-induced generalized seizures in rats. *Brain Res Bull*, 90:52-57.
https://doi.org/10.1016/j.brainresbull.2012.09.007

Persaud A, Jiang C, Liu ZT, et al., 2022. Elevated intracellular Na^+ and osmolarity stimulate catalytic activity of the ubiquitin ligase Nedd4-2. *Proc Natl Acad Sci USA*, 119(30): e2122495119.
https://doi.org/10.1073/pnas.2122495119

Pitzer A, Elijovich F, Laffer CL, et al., 2022. DC ENaC-dependent inflammasome activation contributes to salt-sensitive hypertension. *Circ Res*, 131(4):328-344.
https://doi.org/10.1161/CIRCRESAHA.122.320818

Quansah H, N'Gouemo P, 2014. Amiloride and SN-6 suppress audiogenic seizure susceptibility in genetically epilepsy-prone rats. *CNS Neurosci Ther*, 20(9):860-866.
https://doi.org/10.1111/cns.12296

Scambler T, Jarosz-Griffiths HH, Lara-Reyna S, et al., 2019. ENaC-mediated sodium influx exacerbates NLRP3-dependent inflammation in cystic fibrosis. *Elife*, 8:e49248. https://doi.org/10.7554/eLife.49248

Schlegel A, Mueller M, Muller X, et al., 2023. A multicenter randomized-controlled trial of hypothermic oxygenated perfusion (HOPE) for human liver grafts before transplantation. *J Hepatol*, 78(4):783-793. https://doi.org/10.1016/j.jhep.2022.12.030

Shi XC, Yin YJ, Guo XW, et al., 2023. The histone deacetylase inhibitor SAHA exerts a protective effect against myocardial ischemia/reperfusion injury by inhibiting sodium-calcium exchanger. *Biochem Biophys Res Commun*, 671: 105-115. https://doi.org/10.1016/j.bbrc.2023.05.120

Sitbon A, Delmotte PR, Goumard C, et al., 2023. Therapeutic potentials of mesenchymal stromal cells-derived extracellular vesicles in liver failure and marginal liver graft rehabilitation: a scoping review. *Minerva Anestesiol*, 89(7-8):690-706. https://doi.org/10.23736/S0375-9393.23.17265-8

Tarjus A, González-Rivas C, Amador-Martínez I, et al., 2019. The absence of endothelial sodium channel α (αENaC) reduces renal ischemia/reperfusion injury. *Int J Mol Sci*, 20(13):3132. https://doi.org/10.3390/ijms20133132

Xue J, Zeng WZ, Han Y, et al., 2023. Structural mechanisms of the human cardiac sodium-calcium exchanger NCX1. *Nat Commun*, 14:6181. https://doi.org/10.1038/s41467-023-41885-4

Yu YW, Que JQ, Liu S, et al., 2022. Sodium-glucose co-transporter-2 inhibitor of dapagliflozin attenuates myocardial ischemia/reperfusion injury by limiting NLRP3 inflammasome activation and modulating autophagy. *Front Cardiovasc Med*, 8:768214. https://doi.org/10.3389/fcvm.2021.768214

Zhou ZJ, Chen GS, Si ZZ, et al., 2020. Prognostic factors influencing outcome in adult liver transplantation using hypernatremic organ donation after brain death. *Hepatobiliary Pancreat Dis Int*, 19(4):371-377. https://doi.org/10.1016/j.hbpd.2020.06.003

Supplementary information

Tables S1 and S2